



Research Paper

Construction of a physically cross-linked carrageenan/chitosan/calcium ion double-network hydrogel for 3-Nitro-1, 2, 4-triazole-5-one removal

Lun Huang, Shaohua Jin, Fang Bao, Shuxian Tang, Jueying Yang, Kelin Peng, Yu Chen*

School of Materials Science and Engineering, Beijing Institute of Technology, Beijing 100081, PR China



ARTICLE INFO

Editor: Dr. H. Artuto

Keywords:

Physically crosslinked hydrogels
NTO
Adsorption
Carrageenan
Chitosan

ABSTRACT

3-Nitro-1, 2, 4-triazole-5-one (NTO) is an important insensitive explosive. The discharge of NTO wastewater not only pollutes the environment but also causes the economic loss of the valuable explosive. Currently, the NTO wastewater in industrial production is often treated with activated carbon adsorbents. There are no green, efficient and specific adsorption materials for the NTO treatment yet. In the present work, polymer materials suitable for NTO adsorption were screened by molecular dynamics simulation. With the optimized materials, a carrageenan/chitosan/calcium ion physically cross-linked double network hydrogel (KC/CTS/Ca²⁺ PCDNH) was successfully prepared by the semi-soluble-acidified sol-gel conversion method. The structure and NTO adsorption performance of the hydrogel were investigated by scanning electron microscopy (SEM), Fourier-transform infrared spectroscopy (FTIR), and X-ray photoelectron spectroscopy (XPS). The NTO adsorption kinetics, isotherm, and thermodynamics were further studied to understand the adsorption behavior and mechanism. In addition, the adsorbed NTO was successfully released and recovered by soaking the hydrogel in NaOH solution. Our work has provided an environmentally friendly and targeted preparation method of NTO adsorbent materials for NTO wastewater treatment.

1. Introduction

3-Nitro-1, 2, 4-triazole-5-one (NTO) is an important insensitive energetic material with wide application prospects (Lee et al., 1987). It has been used as primary explosives, polymer based mixed explosives, and energetic catalysts. Compared with traditional explosives, NTO shows better explosive performances and is less sensitive to external stimuli, such as impact, friction, heat, spark, and shock waves (Klapötke and Witkowski, 2016; Trache et al., 2017; Williamson et al., 2016). It is considered a good substitute for traditional explosives (Zhao et al., 2017; Pourmortazavi et al., 2012). However, the increased production of NTO produces large amounts of wastewater containing NTO residues, which has brought severe environmental issues. Studies have shown that NTO wastewater can cause human reproductive diseases (Madeira et al., 2018). In addition, the NTO in wastewater is of great economic value, and the direct discharge also causes huge economic losses.

Currently, the studies of energetic material wastewaters have been mostly focused on TNT wastewater. The treatment of NTO wastewater has only been ongoing in recent years. There are mainly four treatment methods for NTO wastewater, biodegradation, chemical degradation,

phytoremediation, and adsorption. Madeira et al. (2017) successfully degraded the NTO in wastewater in an anaerobic and aerobic microbial environment. However, biodegradation requires strictly controlled environments. Terracciano et al. (2018) were able to chemically degrade the NTO in wastewater with hydrogen peroxide under the irradiation of ultraviolet light. However, irradiation requires certain amounts of energy. RoyChowdhury et al. (2020) purified NTO wastewater by phytoremediation using vetiver that could absorb the NTO in wastewater. This method is suitable for the removal of low concentrations of NTO from wastewater. Fawcett-Hirst et al. (2020) discovered that activated carbon could absorb NTO with high adsorption capacities. Compared with the other treatment methods, adsorption shows more advantages for the treatment of NTO wastewater, such as low cost, simple operation, high efficiency, and high NTO recovery. However, the NTO adsorption of activated carbon is non-specific and the adsorption efficiency is low. In addition, the desorption efficiency of NTO from activated carbon has not been studied and is unclear. Efficient, and green adsorbents for NTO removal and recovery have not been reported yet.

Hydrogel has been demonstrated as an excellent adsorbent for wastewater treatment. In addition to its three-dimensional network

* Corresponding author.

E-mail address: cylsy@163.com (Y. Chen).

structure, various functional groups can also improve the adsorption efficiency by interacting with the harmful substances in wastewater. However, most hydrogel adsorbents are synthesized by polymerization, grafting, and chemical crosslinking, which usually requires high energy consumptions and causes environmental pollutions (Hunt et al., 2011). Natural polymer materials are abundant and cheap (Halake et al., 2016). The hydrogel construction by the physical crosslinking of natural macromolecules avoids the use of toxic chemical crosslinking agents, and thus the hydrogels are considered as a green and safe new adsorption material (Wang et al., 2003). However, the physical interactions for crosslinking, such as single metal ion crosslinking (Morales et al., 2020), hydrogen bonding (Hu et al., 2020), and electrostatic interaction (Li et al., 2016), are weak, which usually produce hydrogels with poor mechanical properties. The hydrogels constructed by dual physical interactions, such as metal ion crosslinking and hydrogen bonding (Liu et al., 2018), metal ion crosslinking and electrostatic action (Tang et al., 2020), or two metal ion cross-linking (Srivastava et al., 2021), exhibit better mechanical properties and adsorption properties and are more practical. Up to now, the hydrogel adsorbents have been mainly used for the treatments of heavy metal ions, dye wastewater and so on (Van et al., 2018). Yet, the physical hydrogel adsorbent for the treatment of energetic material in wastewater is rarely reported (Fawcett-Hirst et al., 2021).

Herein, aiming to explore new treatment methods of energetic material wastewater, we attempted to develop a physically crosslinked hydrogel with natural polymers. First, the raw materials for the hydrogel construction were screened by molecular dynamics simulation. A physically crosslinked natural polymer hydrogel, KC/CTS/Ca²⁺ PCDNH, was then prepared by the semi-soluble-acidified sol-gel conversion. The NTO adsorption and recovery performances of the hydrogel were then evaluated.

2. Materials and methods

2.1. Materials

κ -Carrageenan (KC, AR) was purchased from Shanghai Meryer Chemical Technology Co., Ltd (Shanghai, China). Chitosan (CTS, deacetylation degree, 90%; 230 kDa) was purchased from Zhejiang Aoxing Biotechnology Co., Ltd (Yuhuan, China). Calcium carbonate (CaCO₃, AR), acetic acid (AR), hydrochloric acid (HCl, AR), sodium hydroxide (NaOH, AR), and activated carbon (pharmaceutical grade) were purchased from Beijing Tongguang Fine Chemical Co., Ltd (Beijing, China). 3-nitro-1, 2, 4-triazole-5-one (NTO) was synthesized by nitration reaction of 1, 2, 4-triazole-5-one (TO) in the laboratory (Zhao et al., 2017).

2.2. Molecular dynamics simulation

To select the most suitable raw materials from natural polymers for the preparation of NTO adsorbent, the binding energies between different functional groups and NTO were calculated by molecular dynamics simulation. The polymer containing the functional group with the highest binding energy with NTO was used to prepare hydrogel. The radial distribution function (RDF) of the interaction between the raw material and NTO was further analyzed to explore the NTO adsorption mechanism of the hydrogel.

The force field, convergence level, electrostatic force, and van der Waals are chosen as COMPASS, fine, Ewald, and atom-based, respectively. The detailed calculation process can be found in the [Supplementary Information \(S1\)](#).

2.3. Preparation of KC/CTS/Ca²⁺ PCDNH

Certain amounts of CaCO₃ and deionized water were added into a conical flask and stirred for 10 min. A certain amount of KC was then

Table 1
Compositions of KC/CTS/Ca²⁺ PCDNH.

Sample	Mass fraction (wt%)		
	KC	CTS	CaCO ₃
H1	0.750	1.250	0.125
H2	1.000	1.000	0.125
H3	1.250	1.750	0.125
H4	1.500	0.500	0.125
H5	1.750	0.250	0.125
H6	1.000	1.000	0.025
H7	1.000	1.000	0.075
H8	1.000	1.000	0.175
H9	1.000	1.000	0.225

added into the flask and stirred until it was dissolved. CTS was then added to the KC solution and stirred to form a slurry-like mixture. The slurry was poured into a petri dish, placed in a sealed box containing a certain amount of acetic acid, and allowed to gel for 24 h. The prepared KC/CTS/Ca²⁺ PCDNH was taken out and rinsed with deionized water. The hydrogels with different compositions are listed in [Table 1](#).

2.4. Characterizations

The IR spectra of KC, CTS, and freeze-dried KC/CTS/Ca²⁺ PCDNH were measured with a Bruker ALPHA II FTIR spectrometer (Bruker, Germany) in the range of 4000–400 cm⁻¹ at the resolution of 4 cm⁻¹ for 32 scans.

The KC and freeze-dried KC/CTS/Ca²⁺ PCDNH before and after NTO adsorption were cut into thin slices, dried, and measured for XPS spectra with a PHI QUANTERA-II SXM X-ray photoelectron spectroscope (ULVAC-PHI, Japan). The ray source was Alka (Al target, 1486.6 eV and line width 0.68 eV). The data were fitted by the software MultiPak.

The cross-section morphologies of KC/CTS/Ca²⁺ PCDNH before and after NTO adsorption were imaged with a Phenom Pro scanning electron microscope (Phenom-Scientific, China) at the acceleration voltage of 10 kV. The hydrogel cross-section was fixed on a metal base with conductive tape and sputter-coated with a layer of gold before the test.

The porosity of KC/CTS/Ca²⁺ PCDNH was measured by the method reported in the literature (Kirsebom et al., 2010; Kumari et al., 2016). Briefly, the freeze-dried hydrogel (about 3 mm thick) was cut into 10 mm × 10 mm pieces, weighed, and soaked in 10 mL cyclohexane for 1 h. The hydrogel pieces were then taken out, quickly wiped to remove the cyclohexane on the surface, and weighed. The swelling ratio was calculated with [Eq. \(1\)](#).

$$P = \frac{W_s - W_d}{W_s} \times 100\% \quad (1)$$

Where P (g/g) is porosity, and W_d (g) and W_s (g) are the weights of the hydrogel before and after NTO adsorption, respectively.

The mechanical properties of KC/CTS/Ca²⁺ PCDNH were evaluated with tensile strength and the elongation at break. The samples were respectively cut into dumbbell-shaped strips with the thickness of 2 mm and tested for tensile strength and the elongation at the break on an Instron 6022 Universal Materials Testing Machine (Instron Corporation, USA) at the tensile rate of 100 mm/min.

The rheological properties of KC/CTS/Ca²⁺ PCDNH were characterized with 1 mm thick wafers using a Physica MCR 302 rheometer (Anton Paar GmbH, Germany) at 25 °C. The parallel plate rotor speed was set to 25 PPM, and the strain was 0.1%. The scanning angular frequency was 0.1–100 rad/s (Dev et al., 2020).

The swelling properties of KC/CTS/Ca²⁺ PCDNH were characterized by swelling ratio. The freeze-dried hydrogel was cut into square-shaped pieces with the size of 10 mm × 10 mm × 3 mm, weighed, immersed in the swelling solution, and allowed to swell at 25 °C for 24 h. The pH value of the solution was adjusted with 0.1 M HCl. The swelling ratio

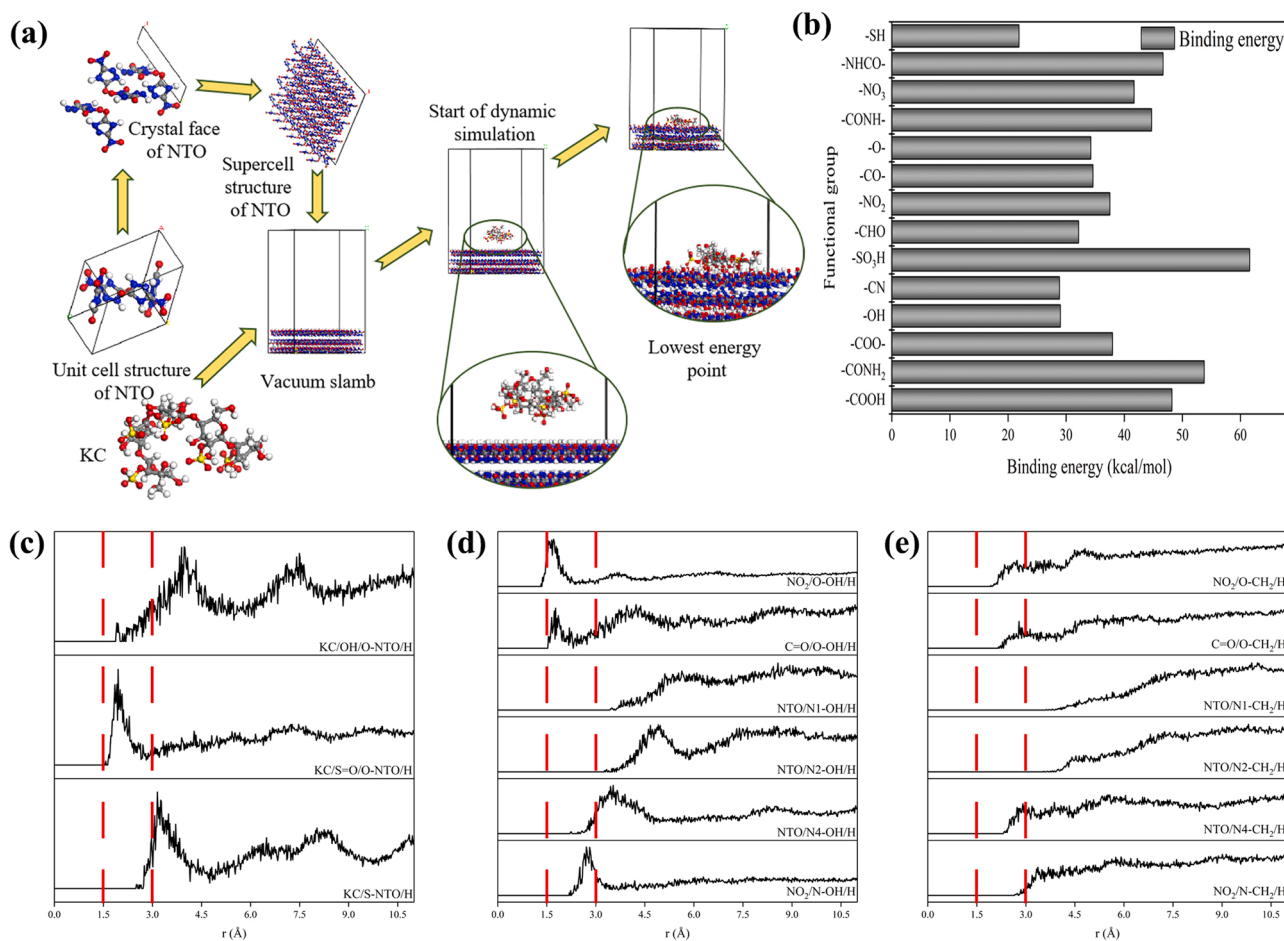


Fig. 1. Molecular dynamics simulation for optimal hydrogel skeleton material. (a) Molecular dynamics simulation process, (b) Binding energies between different functional groups and NTO, (c) Forces between the O and S on KC and the H on NTO, and (d) and (e) Forces between the N and O on NTO and the H on KC.

was calculated with Eq. (2) (Kirsebom et al., 2010; Kumari et al., 2016).

$$S = \frac{W_s - W_d}{W_d} \quad (2)$$

Where S (g/g) is swelling ratio, and W_d (g) and W_s (g) are the weights of the freeze-dried and swollen hydrogel, respectively.

2.5. Adsorption experiments

To study the NTO adsorption behavior and mechanism of KC/CTS/ Ca^{2+} PCDNH, adsorption capacity, adsorption kinetics, adsorption isotherm, and adsorption thermodynamics were systematically studied. The concentration of NTO was determined by measuring the UV absorption at about 320 nm with a TU-1810 UV-Vis spectrophotometer (Pullout General Instrument Co., Ltd., Beijing, China).

2.5.1. Adsorption capacity

To measure the NTO adsorption capacity, 15 mg of freeze-dried KC/CTS/ Ca^{2+} PCDNH was added into a plastic centrifuge tube containing 15 mL of 200 mg/L NTO solution. The adsorption was carried out in a thermostatic oscillator (80 rpm) for 10 h at 298 K. The concentration of NTO solution after adsorption was then measured. The adsorption capacity was calculated with Eq. (3).

$$Q_t = \frac{(C_0 - C_t)V_t}{m} \quad (3)$$

Where Q_t (mg/g) is the adsorption capacity at time t , C_0 (mg/L) is the initial NTO concentration, C_t (mg/L) is NTO concentration in solution at

time t , V_t (L) is the volume of the solution at time t , and m (g) is the weight of the hydrogel.

2.5.2. Adsorption kinetics

To determine the adsorption kinetics, 15 mg of freeze-dried KC/CTS/ Ca^{2+} PCDNH was immersed in 15 mL of NTO solution with the initial concentration of 120 mg/L, 200 mg/L, or 400 mg/L in a plastic centrifuge tube and oscillated at 80 rpm and 298 K. An aliquot of 3 mL was sampled from the supernatant at the pre-set time intervals (0 min, 30 min, 60 min, 120 min, 240 min, 420 min, 660 min) and measured for the concentration of NTO.

2.5.3. Adsorption isotherm

The adsorption isotherm was obtained by respectively immersing 15 mg of freeze-dried KC/CTS/ Ca^{2+} PCDNH samples in 15 mL of 40 mg/L, 120 mg/L, 200 mg/L, 300 mg/L, 400 mg/L, 500 mg/L, and 600 mg/L NTO solutions. The adsorption was conducted under 80 rpm oscillation at the constant temperature of 298 K, 308 K, or 318 K for 10 h. The concentration of NTO in solution was then measured after the adsorption.

2.5.4. NTO desorption

The NTO adsorbed KC/CTS/ Ca^{2+} PCDNH was immersed in 10 mL NaOH solution (pH=10–14) at room temperature for 24 h. The NTO concentration in solution was then determined by measuring the UV absorption at about 410 nm with the UV-Vis spectrophotometer. The desorption capacity was calculated with Eq. (4).

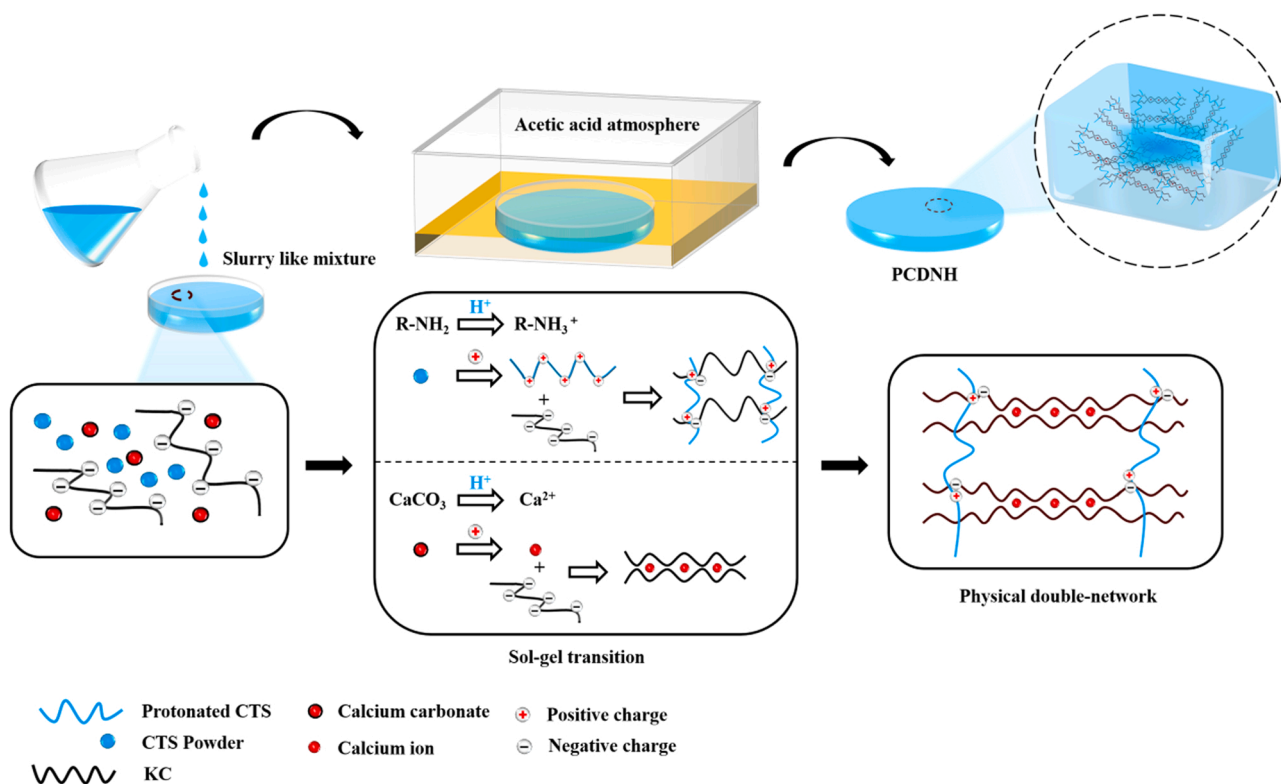


Fig. 2. Formation mechanism of KC/CTS/Ca²⁺ PCDNH.

$$D_t = \frac{C_t V_t}{m Q_m} \times 100\% \quad (4)$$

Where D_t (mg/g) is the desorption capacity at time t , C_t (mg/L) is the concentration of NTO at time t , V_t (L) is the volume of the solution at time t , m (g) is the weight of the hydrogel, and Q_m is the adsorption capacity.

3. Results and discussion

3.1. Construction and characterization of KC/CTS/Ca²⁺ PCDNH

3.1.1. Molecular dynamics simulation

Natural polymers contain many functional groups that can bind NTO differently. To optimize a hydrogel skeleton material with a strong affinity to NTO, the interactions between the functional groups possibly found in 14 kinds of natural polymers and NTO are simulated by molecular dynamics simulation. As shown in Fig. 1a, the binding energy between the sulfonic acid group and NTO is the highest. The bond length is 1.5–3 Å, within the range of hydrogen bond action in the RDF of the interaction force (Liu et al., 2016). Specifically, the hydrogen bonding can occur between the O of the sulfonic acid group in KC and H of NTO, as well as the O of NTO and H of the hydroxyl group in KC (Figs. 1c–1e). Hydrogen bonding is stronger than the intermolecular force, and thus NTO adsorbs on KC mainly via the hydrogen bonding. Therefore, KC containing sulfonic acid group was selected as the hydrogel skeleton material. To construct a physically crosslinked double-network polyelectrolyte composite hydrogel by semi-soluble-acidified sol-gel conversion method, CTS and CaCO₃ were selected as the auxiliary materials.

3.1.2. Formation mechanism of KC/CTS/Ca²⁺ PCDNH

The formation mechanism of KC/CTS/Ca²⁺ PCDNH is depicted in Fig. 2. The hydrogel is prepared by the semi-soluble-acidified sol-gel conversion that has been developed by Zhao et al. (2018) of our research group for the preparation of double-network polyelectrolyte hydrogels.

This method can prevent the precipitation of polyelectrolyte hydrogel caused by the high local concentrations of cations and anions (Luo et al., 2015) and avoid the uneven dispersion of calcium ions that are used to promote the gelation of KC (Prajapati et al., 2014). During the preparation process, the dissolution of anion polyelectrolyte KC increases the solution viscosity, which facilitates the uniform dispersion of the insoluble calcium carbonate and CTS to form a slurry mixture. The mixture is then placed in a sealed plastic container containing acetic acid. The gaseous acetic acid gradually penetrates the mixture, which releases Ca²⁺ from the CaCO₃ and protonates -NH₂ on the CTS to form -NH₃⁺. The CTS gradually dissolves and complexes with KC and Ca²⁺ via PEC interaction to form KC/CTS/Ca²⁺ PCDNH with a complete and uniform three-dimensional structure.

3.1.3. FTIR

Fig. 3a shows the IR spectra of KC, CTS, and CTS/SA/Ca²⁺ PCDNH. Both CTS and KC exhibit their characteristic absorption peaks. In KC/CTS/Ca²⁺ PCDNH, the stretching vibration peak of C=O at 1651 cm⁻¹ and bending vibration peak of N-H at 1588 cm⁻¹ of CTS shift to 1633 cm⁻¹ and 1530 cm⁻¹, respectively (Paiva et al., 2013). The S-O stretching vibration peak in the sulfonic acid group of KC shifts from 1226 cm⁻¹ to 1215 cm⁻¹ (Kulkarni et al., 2011; Selvakumaran et al., 2015). The comparison of the IR spectra of KC+CTS blended powder and KC/CTS/Ca²⁺ PCDNH (Fig. 3b) also suggests that the characteristic absorption peaks of N-H and S-O shift to the low-frequency region in the hydrogel. These results infer that the -NH₂ of CTS is converted into -NH₃⁺ and the electrostatic interaction between the -NH₃⁺ and the sulfonic group of KC forms the double network hydrogel.

3.1.4. XPS

Fig. 3c shows the XPS spectra of KC and the hydrogel. No N 1s is observed in KC because there is no nitrogen, while an obvious N 1s appears as CTS introduced into the hydrogel. The N 1s peak of the hydrogel is deconvoluted into two peaks at 399.48 eV and 401.58 eV which are attributed to the nitrogen of -NH₂ and -NH₃⁺, respectively

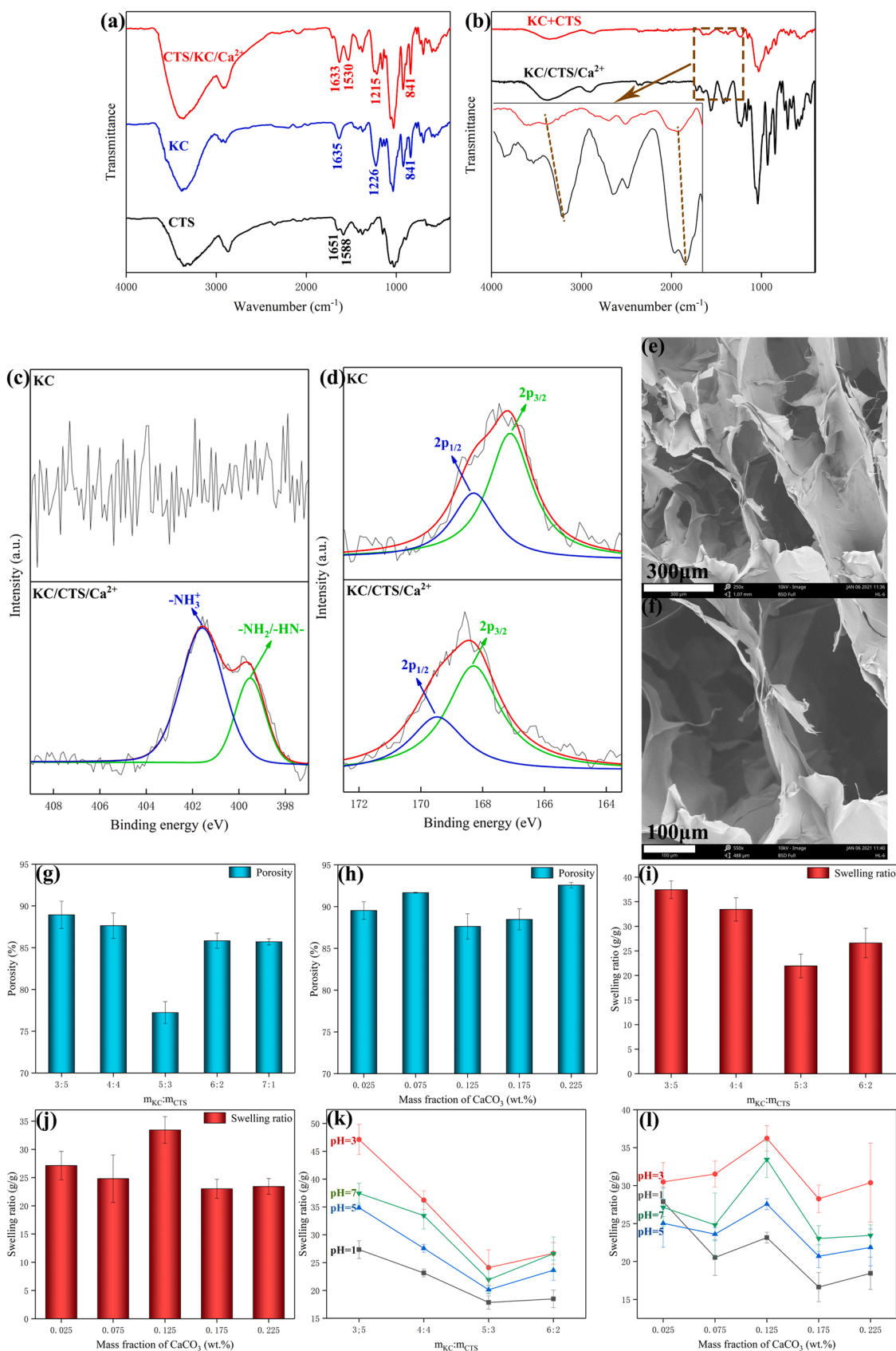


Fig. 3. Structural characterization of KC/CTS/Ca²⁺ PCDNH. (a) IR spectra of KC/CTS/Ca²⁺, KC and CTS, (b) IR spectra of KC+CTS blended powder and KC/CTS/Ca²⁺, (c) N 1s XPS spectra of KC and hydrogel, (d) S 2p XPS spectra of KC and hydrogel, (e) and (f) SEM images at 250 × (e) and 550 × (f) magnifications of KC/CTS/Ca²⁺ PCDNH, and (g-l) Porosities (g and h) and swelling ratios (i-l) of KC/CTS/Ca²⁺ PCDNH prepared at different mass ratios of KC to CTS with different amounts of CaCO₃.

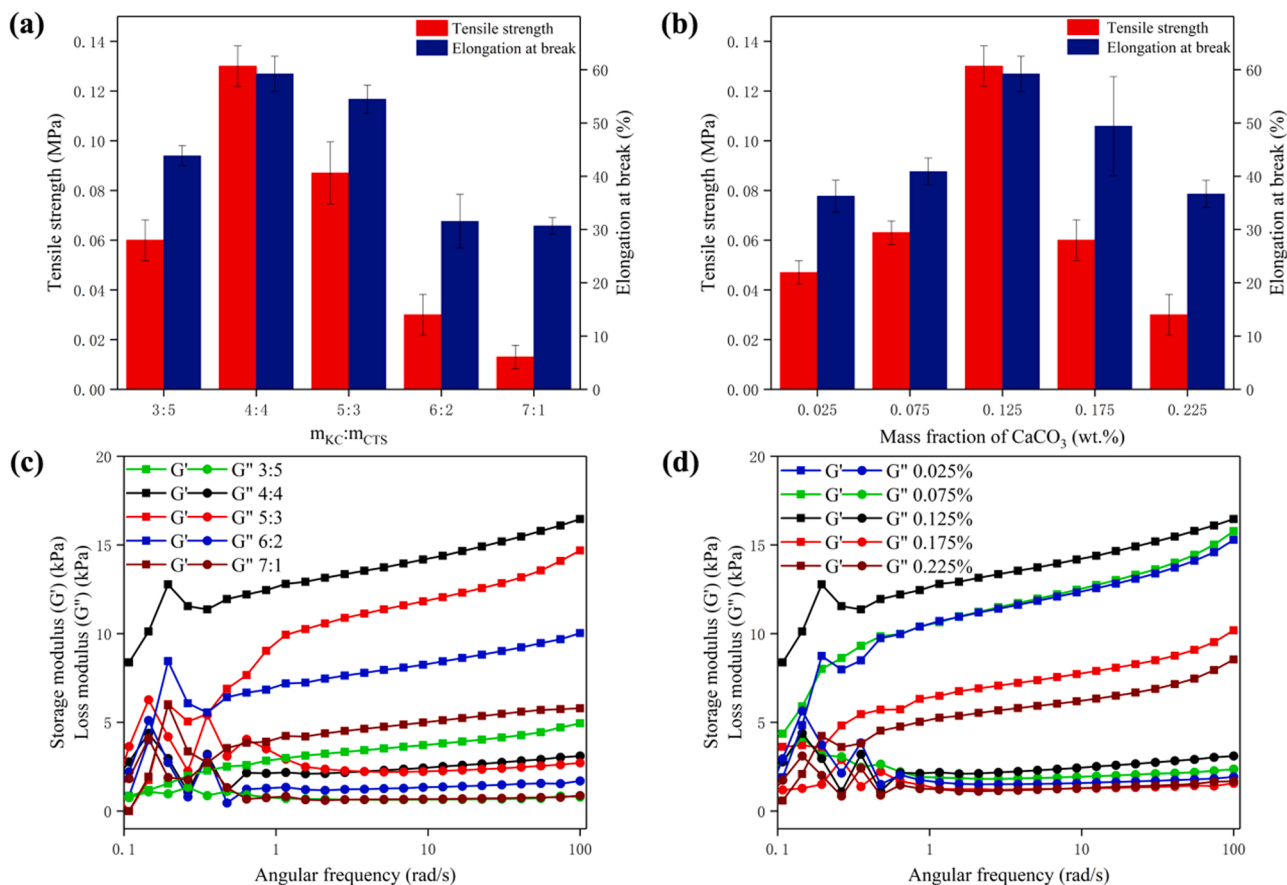


Fig. 4. Mechanical properties (a and c) and rheological properties (b and d) of KC/CTS/Ca²⁺ PCDNH prepared at different mass ratios of KC to CTS with different amounts of calcium carbonate.

(Bratskaya et al., 2007). All the S 2p peaks of KC shift towards the high-energy region in the hydrogel (Fig. 3d). Specifically, the 2p_{1/2} and 2p_{3/2} of KC at 168.27 eV and 167.07 eV respectively shift to 169.48 eV and 168.28 eV in hydrogel. It can be explained that the electrostatic interaction between the sulfonate group in KC and the -NH₃⁺ of CTS increases the steric hindrance of S, and thus the release of S requires higher energy. These results further confirm that the hydrogel is formed via electrostatic interaction.

3.1.5. SEM

Fig. 3e and Fig. 3f show the cross-section morphology of KC/CTS/Ca²⁺ PCDNH. The hydrogel exhibits a layered porous structure with different pore sizes and small holes in the large pores. The porous structure can facilitate NTO diffusion and improve swelling properties. The large surface area of the porous structure offers more adsorption sites, which can also improve the adsorption capacity of the hydrogel.

3.1.6. Porosity

Fig. 3g and Fig. 3h show the porosities of KC/CTS/Ca²⁺ PCDNH samples prepared at different mass ratios of KC to CTS with different amounts of CaCO₃. The polyelectrolyte interaction between KC and CTS is gradually enhanced as the amount of KC increased, which reduces the porosity of hydrogel and forms denser hydrogels. However, extremely high KC contents and low CTS contents are un conducive to the polyelectrolyte complexation and result in crosslinked structures of low densities and high porosities. In addition, with the increase of calcium carbonate mass, the porosity of hydrogels generally decreases at first and then increases. All samples exhibit porosities higher than 75% with the highest value of over 90%. These results further confirm that KC/CTS/Ca²⁺ PCDNH is a porous structure that can provide a large space for

NTO adsorption.

3.1.7. Swelling property

Fig. 3i and Fig. 3j show the swelling properties of KC/CTS/Ca²⁺ PCDNH. The swelling ratios of all samples are over 20 g/g, indicating the good swelling properties of KC/CTS/Ca²⁺ PCDNH. Good swelling properties are beneficial to NTO adsorption. The swelling ratio displays the same changing trend with KC content as porosity. With the increase of KC content, the swelling ratio decreases firstly and then increases, indicating that the swelling behavior is mainly affected by porosity. No swelling data were obtained for the hydrogel prepared at the 7:1 mass ratio of KC to CTS because of its poor mechanical property. The hydrogel was broken during the swelling test.

Fig. 3k and Fig. 3l show the swelling ratios of the KC/CTS/Ca²⁺ PCDNH samples prepared under different conditions at different pHs. As can be seen, the swelling ratios of the hydrogels show similar changing trends with pH. Acidic environments are conducive to swelling to a certain extent, but extremely acidic environments break the hydrogel network due to partial hydrolysis of KC and reduce swelling ratio. NTO wastewater is usually acidic with the pH ranging from 3 to 4 (Xue et al., 2007). The highest swelling ratio of the hydrogel displayed in weakly acidic environment is conducive to NTO adsorption.

3.1.8. Mechanical property

The mechanical property of hydrogel is an important parameter for its application. Good mechanical properties can maintain the structural integrity of the hydrogel in practical applications. Fig. 4a shows the tensile strengths and elongations at the break of KC/CTS/Ca²⁺ PCDNH samples prepared at different mass ratios of KC to CTS. The tensile strength firstly increases and then decreases with the increase of CTS

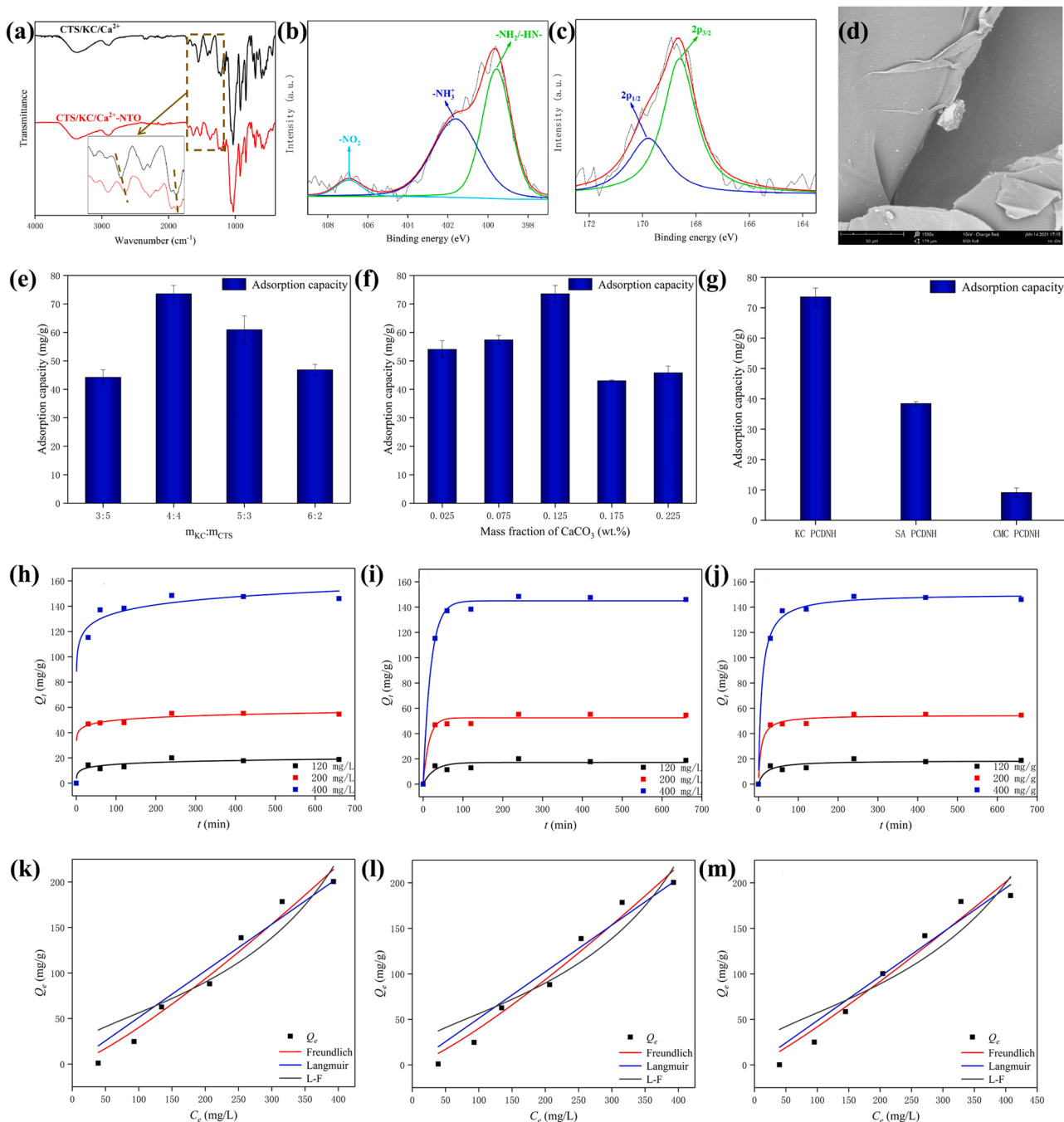


Fig. 5. NTO adsorption properties of KC/CTS/Ca²⁺ PCDNH. (a) IR spectra of KC/CTS/Ca²⁺ PCDNH before and after NTO adsorption; (b, c) N 1s (b) and S 2p (c) XPS spectra of KC/CTS/Ca²⁺ PCDNH after NTO adsorption; (d) 1500 × SEM image of KC/CTS/Ca²⁺ PCDNH after NTO adsorption, (e) Adsorption capacities of the hydrogels prepared at different mass ratios of KC to CTS; (f) Adsorption capacities of the hydrogels prepared with different amounts of CaCO₃; (g) Adsorption capacities of the natural polymer-based hydrogels prepared with CMC, SA, and KC; (h) Elovich model fitting curve; (i) Pseudo-first-order model fitting curve; (j) Pseudo-second-order model fitting curve; (k-m) Fitting curves of Langmuir model, Freundlich model and Langmuir-Freundlich model for the adsorptions at 25 °C (k), 35 °C (l), 45 °C (m).

content. Fig. 4b shows the tensile strengths and elongations at the break of the KC/CTS/Ca²⁺ PCDNH samples prepared with different amounts of CaCO₃. The tensile strength increases at first and then decreases with the increase of the amount of CaCO₃. High amounts of CaCO₃ promote the crosslinking of KC, and thus enhance the degree of crosslinking of the whole hydrogel. However, excessive amounts of CaCO₃ inhibit the crosslinking between KC and CTS, causing low crosslinking degrees of the polyelectrolyte network. Therefore, the double-network structure is partially formed, showing poor mechanical properties. The hydrogel prepared with 0.125% CaCO₃ and 4:4 mass ratio of KC to CTS exhibits

the best mechanical properties. The tensile strength of the prepared KC/CTS/Ca²⁺ PCDNH under the optimal conditions is over 1000 kPa, which meets the adsorption requirements.

3.1.9. Rheological property

Fig. 4c and Fig. 4d show the dynamic rheological test results of KC/CTS/Ca²⁺ PCDNH. In the scanning angular frequency range, their storage moduli (G') are larger than their respective loss moduli (G''), showing the typical rheological behavior of hydrogel, suggesting that these double-network physical hydrogels are highly stable under

shearing. The storage modulus firstly increases and then decreases with the increase of CTS content (Fig. 4c) or the amount of CaCO₃ (Fig. 4d), consistent with the changing trend of mechanical property. These results indicate that the rheological properties of KC/CTS/Ca²⁺ PCDNH are closely related to its degree of crosslinking.

3.2. NTO adsorption of KC/SA/Ca²⁺ PCDNH

3.2.1. Adsorption behaviors and performance

The NTO adsorption of KC/CTS/Ca²⁺ PCDNH was then characterized by FTIR, XPS and SEM. Fig. 5a shows IR spectra of KC/CTS/Ca²⁺ PCDNH before and after NTO adsorption. The absorption peaks of amino cation and sulfonic acid group in the hydrogel shift after NTO adsorption, indicating that NTO adsorbs mainly via the interaction with the sulfonic acid group. The amino cation peak shifts because it is close to the absorption peak of the nitro group of NTO. The peak area ratio of -NH₂/-NH- to -NH₃⁺ increases from 0.47 to 1.30 after NTO adsorption (Fig. 5b), indicating that the number of nitrogen atoms is increased. In addition, a new peak appears at 406.92 eV which can be ascribed to the nitrogen in -NO₂. -NH- and -NO₂ can only be from NTO. The XPS spectra of the hydrogel before and after NTO adsorption reveal that the 2p_{1/2} and 2p_{3/2} peaks of the sulfur shift from 169.48 eV and 168.28–169.82 eV and 168.62 eV, respectively (Fig. 5c). It can be explained that NTO forms a hydrogen bond with the sulfonic acid group, which increases the steric hindrance of the sulfur atom. The SEM image at × 1500 clearly shows the NTO particles adsorbed on the hydrogel (Fig. 5d). These results suggest that KC/CTS/Ca²⁺ PCDNH can absorb NTO.

Fig. 5e shows the adsorption capacities of the KC/CTS/Ca²⁺ PCDNH samples prepared at different mass ratios of KC to CTS. The adsorption capacity first increases and then decreases with the increase of KC content, consistent with the changing trends of mechanic and rheological properties. The maximum adsorption capacity of ~73 mg/g is obtained with the hydrogel prepared with 0.125 wt% CaCO₃, 1 wt% KC and 1 wt% CTS. KC plays a leading role in NTO adsorption. Therefore, the adsorption capacity increases with the increase of KC content. However, due to the strong polarity of NTO, it is partially converted into anion, NTO⁻ as dissolved in water. Decreasing the polycation (CTS) content affects the NTO adsorption capacity of the hydrogel. Therefore, the adsorption capacity of hydrogel decreases as the KC content further increased. In particular, extremely high mass ratios of KC to CTS, for example, 7:1, result in hydrogels with low degrees of crosslinking and poor mechanical properties. The porous structure of the hydrogel breaks during the adsorption process, showing no adsorption. The NTO adsorption capacity of KC/CTS/Ca²⁺ PCDNH also shows a trend of increasing first and then decreasing with the increase of the amount of CaCO₃ (Fig. 5f). Higher degrees of the Ca²⁺ crosslinked KC means fewer free anions, which is conducive to the adsorption of NTO. However, an extremely large crosslinking distance weakens the activity of the sulfonic acid groups on the KC which will mainly form the complexes with Ca²⁺, rather than NTO, resulting in low adsorption capacities.

For comparison purpose, the NTO adsorption test was also conducted on the commercially available activated carbon under the same conditions. The activated carbon exhibit the highest adsorption capacity of 25 mg/g, about 1/3 of that of KC/CTS/Ca²⁺ PCDNH. Based on the molecular dynamics simulation results, polyanion/CTS/Ca²⁺ composite hydrogels were also constructed using sodium carboxymethyl cellulose and alginate as the polyanion, respectively and their NTO adsorption performances were measured. As shown in Fig. 5g, the adsorption capacities of the three hydrogels are in the same order as the binding energies between the functional groups of the skeleton materials and NTO, e.g. sulfonate > carboxy > hydroxyl. These results suggest that molecular dynamics simulation can be used to screen optimal polymer structures for the construction of hydrogels with excellent NTO adsorption performances, and is an effective tool for the rapid construction of functional hydrogels with different adsorption functions.

Table 2

Adsorption kinetics model fitting parameters.

Model	Parameter	Concentration (mg/L)		
		120	200	400
Elovich	$Q_{e,exp}$ (mg/g)	18.72	54.55	145.99
	α (mg/(g·min))	20.24	2.03×10^5	2.16×10^5
	β (g/mg)	0.46	0.31	0.11
Pseudo-first-order	R^2	0.55	0.81	0.75
	$Q_{e,cal}$ (mg/g)	17.09	52.45	144.99
	k_1 (L/min)	0.036	0.069	0.052
Pseudo-second-order	R^2	0.81	0.97	0.99
	$Q_{e,cal}$ (mg/g)	18.54	54.60	150.61
	k_2 (g/(mg·min))	2.98×10^{-3}	2.85×10^{-3}	7.95×10^{-4}
	R^2	0.42	0.67	0.93

3.2.2. Adsorption kinetics

Adsorption kinetics is one of the effective tools for evaluating the efficiency of an adsorbent. The Elovich model, pseudo-first-order model, and pseudo-second-order model are used to fit the kinetic data. The equation of each model is shown in S2, and the fitting results are shown in Table 2. The fitting curves of each model are shown in Figs. 5h–5j.

As can be seen, the squared correlation coefficient of the quasi-first-order dynamics model is the largest and increases with the increase of the concentration of the solution, indicating that the NTO adsorption of KC/CTS/Ca²⁺ PCDNH obeys the quasi-first-order kinetic model and is a physical adsorption process, consistent with the IR and XPS characterization results.

3.2.3. Adsorption isotherm

Adsorption isotherm can be used to understand the interaction between an adsorbent and an adsorbate and explore the adsorption mechanism. Herein, the experimental data were fitted with the Langmuir model, Freundlich model, and Langmuir-Freundlich mode, respectively. The equations of the models are shown in S3.

The fitting curves of the isotherm models are shown in Figs. 5k–5m and the fitting parameters of each model are shown in Table 3. The Freundlich model displays the highest fitting degree (R^2), suggesting that the NTO adsorption of KC/CTS/Ca²⁺ PCDNH is a multi-layer adsorption process on a non-uniform surface. The surface of freeze-dried hydrogel is nonuniform, and there is more than one active site for the hydrogen bonding between KC and NTO (Slcopp, 2009). Hydrogen bonds can be formed between the O on KC sulfonic acid group and the H on NTO, as well as between the O on the nitro and -CO₂H of NTO and the H of the -OH of KC, as demonstrated by molecular dynamics simulation.

3.2.4. Adsorption thermodynamics

The adsorption thermodynamic parameters for the NTO adsorption of KC/CTS/Ca²⁺ PCDNH are shown in Table 4. The detailed calculation process of the thermodynamic parameters is shown in S4. The ΔG^0 at all test temperatures is negative, indicating that the adsorption is spontaneous.

3.2.5. NTO desorption

The NTO adsorbed KC/CTS/Ca²⁺ PCDNH was soaked in a NaOH solution to release NTO. Fig. 6a shows the desorption ratios of the hydrogel at different pHs. The NTO is effectively desorbed in strong alkaline solution (pH ≥ 12) with the maximum desorption rate of ~78%. The UV absorption spectra suggest that the desorbed NTO is transformed into Na(NTO)·H₂O (Li et al., 2013) during the desorption process, and thus the hydrogen bond between the hydrogel and NTO is broken. It is also noted that the internal porous structure collapses and the smooth surface becomes rough after the desorption (Figs. 6b and 6c). Therefore, the desorption of NTO with NaOH destroys the three-dimensional

Table 3
Fitting parameters of adsorption isotherm models.

Model	Parameter	Temperature (K)		
		298	308	318
Langmuir	Q_m (mg/g)	5.76×10^5	4.98×10^5	2.06×10^6
	K_L (L/mg)	8.89×10^{-7}	1.34×10^{-6}	3.35×10^{-7}
	R^2	0.95	0.97	0.95
	R_L	0.99947–0.99996	0.99920–0.99995	0.99986–0.99999
Freundlich	K_F ((mg/g)(L/mg) $^{1/n}$)	0.14	0.26	0.23
	n_F	0.82	0.86	0.88
	R^2	0.97	0.98	0.96
Langmuir-Freundlich	K_{LF} ((mg/g)(mg/L) $^{-1/n_{LF}}$)	-0.34	-0.30	-0.057
	a_{LF} ((mg/L) $^{-1/n_{LF}}$)	-1.02	-1.01	-1.00
	n_{LF}	0.0032	0.0022	0.00051
	R^2	0.88	0.90	0.86

Table 4
Thermodynamic parameters for the NTO adsorption of KC/CTS/Ca $^{2+}$ PCDNH.

Temperature (K)	ΔG^0 (kJ/mol)	ΔS^0 (J/mol·K)	ΔH^0 (kJ/mol)
298	-4.33	13.59	-0.28
308	-4.65	14.19	
318	-4.60	13.58	

structure of the hydrogel. The XPS analysis suggests that the NTO desorbed hydrogel contains a large amount of Na 1s (1070 eV) (Erdogan et al., 2021), and the N 1s (399 eV) disappear (Fig. 6d), suggesting that NaOH also reacts with CTS, in addition to NTO. The reaction of NaOH with the $-\text{NH}_3^+$ of CTS breaks the hydrogel and releases NTO. The successful NTO desorption suggests that KC/CTS/Ca $^{2+}$ PCDNH can be used

to recover the high-value and high-performance elite-substance explosive NTO with cheap and environment-friendly natural polymers and thus it is a green, efficient and low-cost treatment and recovery method of high-value explosive wastewater.

4. Conclusions

In summary, the binding energies between functional groups found in natural polymers and NTO were calculated with molecular dynamics simulation. carrageenan, a natural macromolecule containing sulfonic acid groups, was selected as the skeleton material to construct KC/CTS/Ca $^{2+}$ PCDNH adsorbent by the semi-soluble-acidified sol-gel conversion method for NTO adsorption. IR and XPS analyses suggest that the physically crosslinked double network KC/CTS/Ca $^{2+}$ hydrogel is

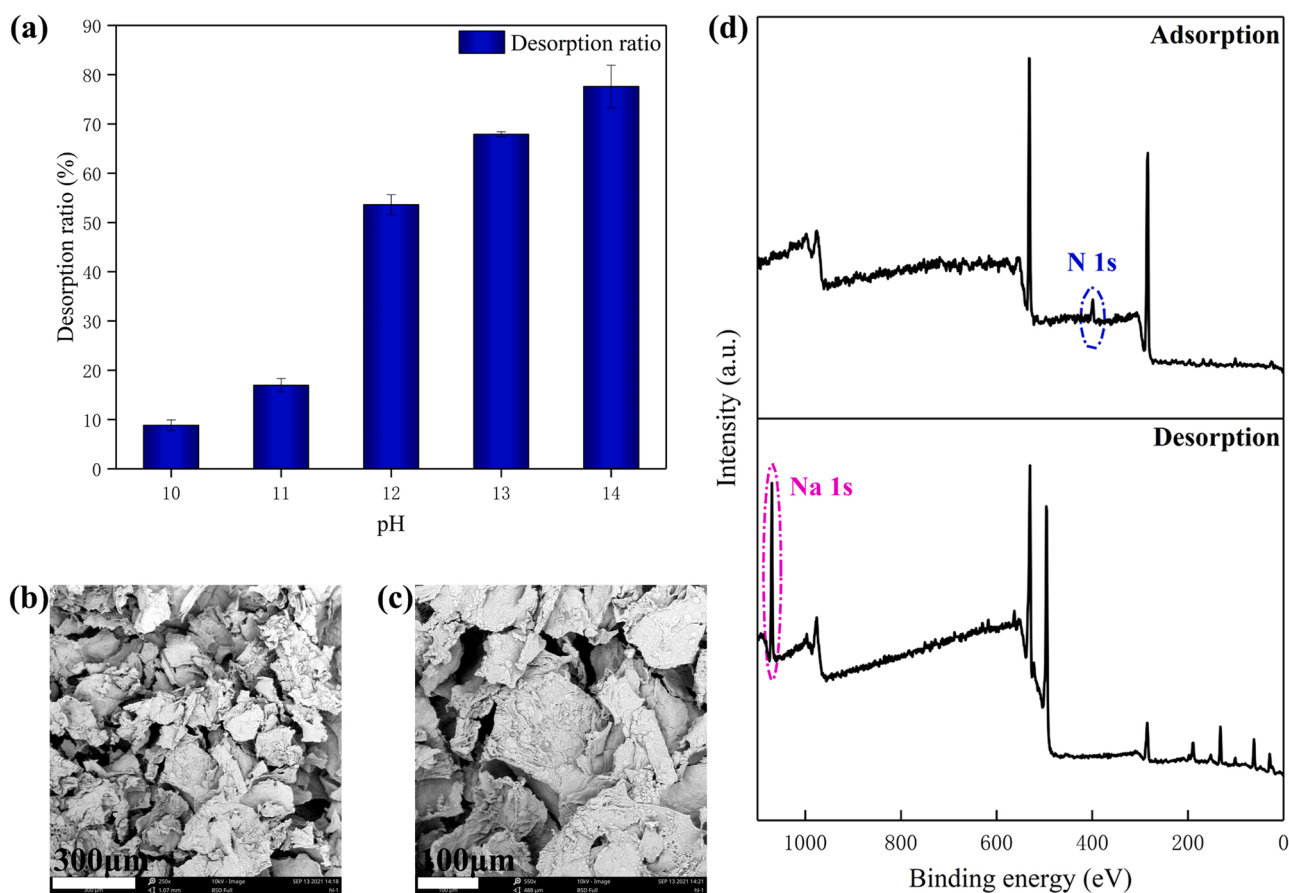


Fig. 6. NTO desorption properties of KC/CTS/Ca $^{2+}$ PCDNH. (a) NTO desorption ratios at different pHs; (b) 250 \times and (c) 550 \times SEM image of KC/CTS/Ca $^{2+}$ PCDNH after NTO desorption; and (d) XPS wide-scan spectra of KC/CTS/Ca $^{2+}$ PCDNH before and after NTO desorption.

composed of the physically cross-linked KC/CTS and KC/Ca²⁺ networks. The hydrogel exhibits good mechanical properties and the porosity of 80–90%. The porous structure provides a large specific surface area for swelling and NTO adsorption. Further investigation suggests that the NTO adsorption of the hydrogel is mainly realized by hydrogen bonding, consistent with the RDF of the interaction force between KC and NTO in molecular dynamics simulation. The maximum NTO adsorption capacity of the hydrogel is determined to be about 73 mg/g. The adsorption process obeys the pseudo-first-order kinetic model and thus is a physical adsorption. The adsorption isotherm satisfies the Freundlich model and ΔG^0 is less than 0, indicating that the adsorption is spontaneous. In addition, the adsorbed NTO is successfully released and recycled from the hydrogel with NaOH solution. In all, a natural polymer-based physically crosslinked double-network hydrogel with excellent NTO adsorption performances has been prepared by the semi-solution-acidification sol-gel conversion method with the assist of the materials optimization by molecular dynamics simulation. Our work has provided an environmentally friendly and targeted preparation method of the adsorbent materials for the treatment of energy-containing wastewaters, showing great application potentials and guiding significances.

CRedit authorship contribution statement

The work presented here was carried out in collaboration with all authors. **Lun Huang**: Experiment and data analysis, Writing – Original draft preparation. **Shaohua Jin**: Conceptualization and methodology. **Fang Bao**: Experiment and data curation. **Shuxian Tang**: Methodology and corrigendum. **Jueying Yang**: Visualization, Writing – reviewing & editing. **Kelin Peng**: Software and validation. **Yu Chen**: Corresponding author. Supervision and methodology, Writing – reviewing & editing.

Declaration of Competing Interest

The authors declare that they have no known competing financial interests or personal relationships that could have appeared to influence the work reported in this paper.

Acknowledgments

This work was financially sponsored by the startup fund of medical & engineering integration science and technology project of Beijing Institute of Technology, China.

Appendix A. Supporting information

Supplementary data associated with this article can be found in the online version at [doi:10.1016/j.jhazmat.2021.127510](https://doi.org/10.1016/j.jhazmat.2021.127510).

References

- Bratskaya, S., Marinin, D., Simon, F., Synytska, A., Zschoche, S., Busscher, H.J., Jager, D., van der Mei, H.C., 2007. Adhesion and viability of two enterococcal strains on covalently grafted chitosan and chitosan/ κ -carrageenan multilayers. *Biomacromolecules* 8, 2960–2968. <https://doi.org/10.1021/bm700620j>.
- Dev, A., Mohanbhai, S.J., Kushwaha, A.C., Sood, A., Sardoiwala, M.N., Choudhury, S.R., Karmakar, S., 2020. κ -carrageenan-C-phycoerythrin based smart injectable hydrogels for accelerated wound recovery and real-time monitoring. *Acta Biomater.* 109, 121–131. <https://doi.org/10.1016/j.actbio.2020.03.023>.
- Erdogan, N.H., Kutlu, T., Sedefoglu, N., Kavak, H., 2021. Effect of Na doping on microstructures, optical and electrical properties of ZnO thin films grown by sol-gel method. *J. Alloy. Compd.* 881, 160554 <https://doi.org/10.1016/j.jallcom.2021.160554>.
- Fawcett-Hirst, W., Temple, T.J., Ladyman, M.K., Coulon, F., 2020. Adsorption behaviour of 1,3,5-trinitroperhydro-1,3,5-triazine, 2,4-dinitroanisole and 3-nitro-1,2,4-triazol-5-one on commercial activated carbons. *Chemosphere* 255, 126848. <https://doi.org/10.1016/j.chemosphere.2020.126848>.
- Fawcett-Hirst, W., Temple, T.J., Ladyman, M.K., Coulon, F., 2021. A review of treatment methods for insensitive high explosive contaminated wastewater. *Heliyon* 7, e07438. <https://doi.org/10.1016/j.heliyon.2021.e07438>.
- Halake, K., Kim, H.J., Birajdar, M., Kim, B.S., Bae, H., Lee, C.C., Kim, Y.J., Kim, S., Ahn, S., An, S.Y., Jung, S.H., Lee, J., 2016. Recently developed applications for

- natural hydrophilic polymers. *J. Ind. Eng. Chem.* 40, 16–22. <https://doi.org/10.1016/j.jiec.2016.06.011>.
- Hu, X., Yan, L., Wang, Y., Xu, M., 2020. Smart and functional polyelectrolyte complex hydrogel composed of salean and chitosan lactate as superadsorbent for decontamination of nickel ions. *Int. J. Biol. Macromol.* 165, 1852–1861. <https://doi.org/10.1016/j.ijbiomac.2020.10.039>.
- Hunt, J.N., Feldman, K.E., Lynd, N.A., Deek, J., Campos, L.M., Spruell, J.M., Hernandez, B.M., Kramer, E.J., Hawker, C.J., 2011. Tunable, high modulus hydrogels driven by ionic coacervation. *Adv. Mater.* 23, 2327–2331. <https://doi.org/10.1002/adma.201004230>.
- Kirsebom, H., Topgaard, D., Galaev, I.Y., Mattiasson, B., 2010. Modulating the porosity of cryogels by influencing the nonfrozen liquid phase through the addition of inert solutes. *Langmuir* 26, 16129–16133. <https://doi.org/10.1021/la102917c>.
- Klapötke, T.M., Witkowski, T.G., 2016. Covalent and ionic insensitive high-explosives. *Propellants, Explos. Pyrotech.* 41, 470–483. <https://doi.org/10.1002/prep.201600006>.
- Kulkarni, R.V., Baraskar, V.V., Setty, C.M., Sa, B., 2011. Interpenetrating polymer network matrices of sodium alginate and carrageenan for controlled drug delivery application. *Fibers Polym.* 12, 352–358. <https://doi.org/10.1007/s12221-011-0352-5>.
- Kumari, J., Karande, A.A., Kumar, A., 2016. Combined effect of cryogel matrix and temperature-reversible soluble-insoluble polymer for the development of in vitro human liver tissue. *ACS Appl. Mater. Interfaces* 8, 264–277. <https://doi.org/10.1021/acsmi.5b08607>.
- Lee, K., Chapman, L.B., Cobura, M.D., 1987. 3-Nitro-1,2,4-triazol-5-one, a less sensitive explosive. *J. Energy Mater.* 5, 27–33. <https://doi.org/10.1080/07370658708012347>.
- Li, F., Wang, X., Yuan, T., Sun, R., 2016. A lignosulfonate-modified graphene hydrogel with ultrahigh adsorption capacity for Pb(II) removal. *J. Mater. Chem. A* 4, 11888–11896. <https://doi.org/10.1039/c6ta03779h>.
- Li, N., Zhao, F.Q., Gao, H.X., Hu, R.Z., Xiao, L.B., Yao, E.G., Huang, X.P., Chang, P., 2013. Thermokinetics of the formation reactions of metal (Li, Na, Pb, Cu) salts of 3-nitro-1,2,4-triazol-5-one. *Acta Phys. - Chim. Sin.* 29, 2101–2106. <https://doi.org/10.3866/PKU.WHXB201307153>.
- Liu, C., Liu, H., Xiong, T., Xu, A., Pan, B., Tang, K., 2018. Graphene oxide reinforced alginate/PVA double network hydrogels for efficient dye removal. *Polymers* 10, 835. <https://doi.org/10.3390/polym10080835>.
- Liu, N., Li, Y.N., Zeman, S., Shu, Y.J., Wang, B.Z., Zhou, Y.S., Zhao, Q.L., Wang, W.L., 2016. Crystal morphology of 3,4-bis(3-nitrofurazan-4-yl)furoxan (DNTE) in a solvent system: molecular dynamics simulation and sensitivity study. *CrystEngComm* 18, 2843–2851. <https://doi.org/10.1039/c6ce00049e>.
- Luo, F., Sun, T.L., Nakajima, T., Kurokawa, T., Zhao, Y., Sato, K., Ihsan, A.B., Li, X., Gong, H., Gong, J.P., 2015. Oppositely charged polyelectrolytes form tough, self-healing, and rebuildable hydrogels. *Adv. Mater.* 27, 2722–2727. <https://doi.org/10.1002/adma.201500140>.
- Madeira, C.L., Field, J.A., Simonich, M.T., Tanguay, R.L., Chorover, J., Sierra-Alvarez, R., 2018. Ecotoxicity of the insensitive munitions compound 3-nitro-1,2,4-triazol-5-one (NTO) and its reduced metabolite 3-amino-1,2,4-triazol-5-one (ATO). *J. Hazard. Mater.* 343, 340–346. <https://doi.org/10.1016/j.jhazmat.2017.09.052>.
- Madeira, C.L., Speet, S.A., Nieto, C.A., Abrell, L., Chorover, J., Sierra-Alvarez, R., Field, J.A., 2017. Sequential anaerobic-aerobic biodegradation of emerging insensitive munitions compound 3-nitro-1,2,4-triazol-5-one (NTO). *Chemosphere* 167, 478–484. <https://doi.org/10.1016/j.chemosphere.2016.10.032>.
- Morales, A., Labidi, J., Gullón, P., 2020. Effect of the formulation parameters on the absorption capacity of smart lignin-hydrogels. *Eur. Polym. J.* 129, 109631 <https://doi.org/10.1016/j.eurpolymj.2020.109631>.
- Paiva, D., Ivanova, G., Do Carmo Pereira, M., Rocha, S., 2013. Chitosan conjugates for DNA delivery. *Phys. Chem. Chem. Phys.* 15, 11893–11899. <https://doi.org/10.1039/c3cp51215k>.
- Pourmortazavi, S.M., Rahimi-Nasrabadi, M., Kohsari, I., Hajimirsadeghi, S.S., 2012. Non-isothermal kinetic studies on thermal decomposition of energetic materials. *J. Therm. Anal. Calorim.* 110, 857–863. <https://doi.org/10.1007/s10973-011-1845-6>.
- Prajapati, V.D., Maheriya, P.M., Jani, G.K., Solanki, H.K., 2014. Carrageenan: a natural seaweed polysaccharide and its applications. *Carbohydr. Polym.* 105, 97–112. <https://doi.org/10.1016/j.carbpol.2014.01.067>.
- RoyChowdhury, A., Mukherjee, P., Panja, S., Datta, R., Christodoulatos, C., Sarkar, D., 2020. Evidence for phytoremediation and phytoexcretion of NTO from industrial wastewater by vetiver grass. *Molecules* 26, 74. <https://doi.org/10.3390/molecules26010074>.
- Selvakumaran, S., Muhamad, I.I., 2015. Evaluation of kappa carrageenan as potential carrier for floating drug delivery system: effect of cross linker. *Int. J. Pharm.* 496, 323–331. <https://doi.org/10.1016/j.ijpharm.2015.10.005>.
- Slocpp, J., 2009. Derivation of the freundlich adsorption isotherm from kinetics. *J. Chem. Educ.* 86, 1341–1343. <https://doi.org/10.1021/ed086p1341>.
- Srivastava, A., Kumari, M., Prasad, K.S., 2021. Hydrogel beads containing ginger extract mediated nano-zirconium as an adsorbent for fluoride removal from aqueous solution. *Int. J. Environ. Anal. Chem.* 101, 1–15. <https://doi.org/10.1080/03067319.2021.1877282>.
- Tang, S., Yang, J., Lin, L., Peng, K., Chen, Y., Jin, S., Yao, W., 2020. Construction of physically crosslinked chitosan/sodium alginate/calcium ion double-network hydrogel and its application to heavy metal ions removal. *Chem. Eng. J.* 393, 124728 <https://doi.org/10.1016/j.cej.2020.124728>.
- Terracciano, A., Christodoulatos, C., Koutsospyros, A., Zheng, Z., Su, T.L., Smolinski, B., Arienti, P., Meng, X., 2018. Degradation of 3-nitro-1,2,4-triazole-5-one (NTO) in

- wastewater with UV/H₂O₂ oxidation. *Chem. Eng. J.* 354, 481–491. <https://doi.org/10.1016/j.cej.2018.07.216>.
- Trache, D., Klapötke, T.M., Maiz, L., Abd-Elghany, M., DeLuca, L.T., 2017. Recent advances in new oxidizers for solid rocket propulsion. *Green Chem.* 19, 4711–4736. <https://doi.org/10.1039/c7gc01928a>.
- Van Tran, V., Park, D., Lee, Y.C., 2018. Hydrogel applications for adsorption of contaminants in water and wastewater treatment. *Environ. Sci. Pollut. Res.* 25, 24569–24599. <https://doi.org/10.1007/s11356-018-2605-y>.
- Williamson, D.M., Gymer, S., Taylor, N.E., Walley, S.M., Jardine, A.P., Glauser, A., French, S., Wortley, S., 2016. Characterisation of the impact response of energetic materials: observation of a low-level reaction in 2,6-diamino-3,5-dinitropyrazine-1-oxide (LLM-105). *RSC Adv.* 6, 27896–27900. <https://doi.org/10.1039/c6ra03096c>.
- Xue, H., Gao, H., Twamley, B., Shreeve, J.M., 2007. Energetic salts of 3-nitro-1,2,4-triazole-5-one, 5-nitroaminotetrazole, and other nitro-substituted azoles. *Chem. Mater.* 19, 1731–1739. <https://doi.org/10.1021/cm062964g>.
- Zhao, J., Chen, Y., Yao, Y., Tong, Z.R., Li, P.W., Yang, Z.M., Jin, S.H., 2018. Preparation of the polyelectrolyte complex hydrogel of biopolymers via a semi-dissolution acidification sol-gel transition method and its application in solid-state supercapacitors. *J. Power Sources* 378, 603–609. <https://doi.org/10.1016/j.jpowsour.2018.01.005>.
- Zhao, Y., Chen, S., Jin, S., Li, Z., Zhang, X., Wang, L., Mao, Y., Guo, H., Li, L., 2017. Heat effects of NTO synthesis in nitric acid solution. *J. Therm. Anal. Calorim.* 128, 301–310. <https://doi.org/10.1007/s10973-016-5912-x>.